Substrate Integrated Waveguide-Fed Tapered Slot Antenna With Smooth Performance Characteristics Over an Ultra-Wide Bandwidth

Lisa S. Locke [1,2], Jens Bornemann [1], and Stéphane Claude [2]

[1] Department of Electrical Engineering
University of Victoria, Victoria, BC V8W 3P6, Canada
lsl@uvic.ca, j.bornemann@ieee.org

[2] Herzberg Institute of Astrophysics, Victoria, BC, V9E 2E7, Canada
Stéphane.Claude@nrc-cnrc.gc.ca

Abstract ─ We present an ultra-wide extended K-band (18 GHz – 30 GHz) planar linear tapered slot antenna (LTSA) design. From a parametric study involving eight designs, the best compromise LTSA is selected in terms of flattest gain and beam width and most symmetric beam width. The design is antipodal with alumina (ε_r = 10) substrate and fed with substrate integrated waveguide (SIW). Regular corrugations improve cross-polarization, input return loss, and gain. Numerical simulations use finite element analysis and time domain finite integration technique field solvers. The resulting design has half power beam widths (HPBW) of only $\pm$ 3.2° and $\pm$ 2.5° variation in frequency in the E- and H-planes, respectively. Cross-polarization levels at boresight are 35.7 dB at 18 GHz and 17.4 dB at 30 GHz, return loss is better than -11.7 dB and gain is 9.23 dB with $\pm$ 0.40 dB variation with frequency. Alternatively, for imaging systems requiring efficient illumination of a reflector or focusing elements, a second resulting design shows near-perfect beam symmetry with $HPBW_E/HPBW_H$ = 0.91. These two LTSAs are good candidates for dual-polarization focal plane array feed applications in astronomy imaging.

Index Terms ─ Antipodal tapered slot antenna, beam width, gain, polarization, substrate integrated waveguide, and ultra-wideband.

I. INTRODUCTION

Microwave and millimeter wave astronomy telescopes with mature low noise single pixel receivers are being upgraded with focal plane arrays for faster survey speeds at lower manufacturing costs. This step in instrumentation requires a low-profile, compact, and easily-fabricated antenna element to incorporate into a dual-polarized array, which has been accomplished for general phased arrays [1] and more recently for radio astronomy in the L Band (1 GHz - 2 GHz) [2, 3]. Looking ahead to higher frequencies, it is required to determine a suitable antenna element and array architecture to allow for a two dimensional densely packed array, having a feeding structure with appropriate impedance match, with the capability to work at millimeter wavelengths and active component integration. A planar imaging array in the ultra-wide extended K-band (18 GHz – 30 GHz) will demonstrate suitable antenna architecture and feeding type for use in conjunction with reflectors for an astronomy millimeter wave focal plane array.

An ideal antenna element for this application is the tapered slot antenna (TSA) because it is highly directive and compact. Gibson's TSA antenna [4], termed "Vivaldi" is a planar end fire antenna with an exponential taper. The electromagnetic wave propagates along the increasingly separated metalized tapers until the distance between the edges is large enough to allow wave separation from the antenna structure and thus radiation occurs. An early comprehensive study [5] of the TSA element illustrates the beam width and the impedance effects of various dielectric substrates and taper shapes. A follow-up investigation of the arrays of the TSA elements [6] introduces the important concept of effective dielectric thickness, t_{eff}, and the recommended range of t_{eff} to ensure the

main beam integrity. Due to its planar nature and narrow width, the TSA elements can be placed with minimal transverse spacing without adversely affecting the performance.

Due to its popularity and ease of planar circuit integration, there are other variations beside the linear TSA and the Vivaldi antenna, which include the continuous width slot antenna (CWSA), bunny-ear or balanced antipodal Vivaldi antenna (BAVA) [7], and the Fermi antenna [8]. Moreover, number of different feed structures for TSAs are presented. For the antipodal TSA, a microstrip feed is an easy and obvious choice. In the millimeter wave range, however, microstrip technology is increasingly lossy and, therefore, such designs do not lend themselves to be scaled to 100 GHz applications. Thus, they are usually used in the lower Gigahertz frequency range [9, 10]. A uniplanar TSA can be fed by a coplanar waveguide (CPW) circuit. However, such a feed is narrowband and requires a number of tuning slots [11], whose sizes and configurations are not well suited for in line feeding techniques at millimeter wave frequencies. The wire model of the TSA presented in [12] is interesting, especially including the use of reflector elements, but this technique, in a millimeter wave printed circuit version, will experience the same high losses as the microstrip technology.

Therefore, our proposed feed structure is a substrate integrated waveguide (SIW) [13], an innovative planar transmission line paradigm that allows for waveguide like transmission and offers a compromise between bulky expensive waveguide and lossy planar microstrip. The SIW performs as a planar waveguide, with substrate metalized on both top and bottom surfaces and is flanked by two parallel arrays of circular via holes, which allows for a contained propagating wave. Short SIW transitions to microstrip [14] or coplanar waveguide [15] are provided for integration with MMICs. The combination of planar antipodal LTSA elements and SIW feeding structure is ideally suited for array imaging systems due to its compact nature, high gain, and excellent beam symmetry and frequency scalability above 100 GHz.

The antipodal LTSA with SIW feed, as shown in Fig. 1, has flared metallic faces on opposite sides of the alumina substrate matching the two conductor SIW feed perfectly. In the SIW, the electric field is oriented perpendicular to the substrate as shown in the bottom view of Fig. 1.

This is similar to the fundamental mode in an all-dielectric waveguide. As the top and bottom metallization begin to flare, the electric field, due to the changing boundary conditions, is slowly rotated to be parallel with the substrate in the antenna aperture. Note that this transition is extremely wideband and covers the entire fundamental mode range of the feeding substrate integrated waveguide.
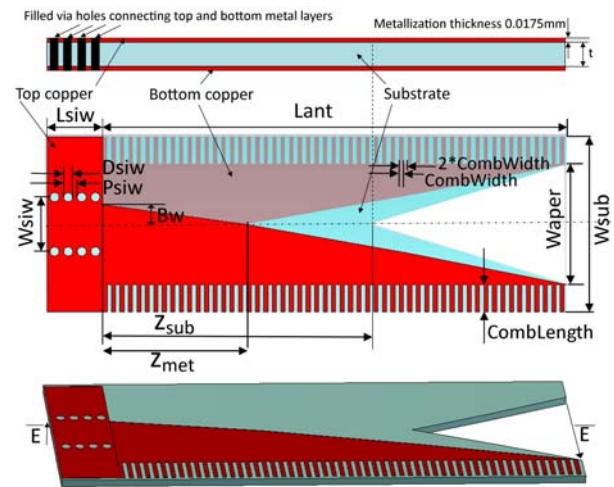

Fig. 1. Antipodal LTSA with SIW feed with a cross sectional view showing top copper metal layer, substrate, bottom copper metal layer, and metal filled via holes that electrically connect top and bottom layers. A Plan view is presented with slightly transparent substrate, and a perspective view. The antenna is sensitive to the horizontal E-fields across the aperture; the antipodal flares rotate the E-vector to a vertical E-field at the SIW feed.

Antipodal LTSAs have poor cross-polarization performance [16] due to the non-zero transverse distance between the metal faces allowing the small unwanted perpendicular (cross-polar) component to the co-polar field. To remedy this, comb-like corrugations are cut out of the metalized layers along the antenna's outside length to improve the main beam shape and reduce sidelobe levels [17].

In this paper, we propose additional benefits of corrugations, which includes improved cross-polarization, reduced VSWR ,and increased on-axis gain. We demonstrate over the extended K-band frequency range of 18 GHz - 30 GHz a constant beam width, constant gain TSA utilizing side corrugations that significantly improve the cross-polarization performance and the input return loss.

II. DESIGN

The antipodal TSA with SIW feed input is shown in Fig. 1. The alumina substrate has copper top and bottom faces and a triangular cut at the aperture end to reduce the discontinuity between the substrate and the free space, thus improving the input return loss. Along the outside edges of the antenna regular comb-like corrugations are cut into the metallized top and bottom layers.

The substrate, 0.381 mm alumina ceramic (Al_2O_3), has excellent thermal conductivity; 31 W/mK at 20°C for active component heat dissipation and a high mechanical strength. The high relative permittivity $\varepsilon_r = 10$ is needed to reduce the total width of the SIW feed by sqrt(ε_r). Since a focal plane array is intended, the distance between each antenna should be $W_{sub} \leq \lambda_0/2$ to avoid grating lobes [6]. The integrated antipodal antenna and feed structure is displayed in Fig. 1 and the dimensions are listed in Table 1.

Table 1: LTSA and feed parameters.

W_{siw}	Via hole center-to-center spacing in y-direction	3.6 mm
D_{siw}	Via hole diameter	0.6 mm
P_{siw}	Via hole center-to-center spacing in z-direction	0.9 mm
L_{siw}	Length of SIW feeding section	3.7 mm
Bw	Distance from center to start of metalized flare	1.3 mm
Comb-width	Corrugation width in z-direction	0.28 mm
t	Thickness of substrate	0.381 mm
ε_r	Relative permittivity of ceramic alumina (Al_2O_3)	10
W_{siweff}	Equivalent waveguide width	3.138mm

Yngvesson in [6] provides a general formula for the effective substrate thickness, $t_{eff} = t*$sqrt($\varepsilon_r - 1$) and the optimum range is normalized to free space wavelength λ_0 for main lobe integrity and low sidelobes,

$$0.005 < t_{eff} / \lambda_0 < 0.03. \qquad (1)$$

Despite being above this range, at $t_{eff}/\lambda_0 = 0.049, 0.082$ for 18 GHz and 30 GHz, respectively, the main beam and sidelobes are acceptable. For future arrays at higher frequencies, the inequality will be more difficult to satisfy and will largely determine the type of dielectric required. Figure 2 plots the upper and lower bounds of equation (1) as a function of frequency for two dielectrics, Rogers RT/Duroid 5880 and alumina, $\varepsilon_r = 2.94$ and 10, respectively.
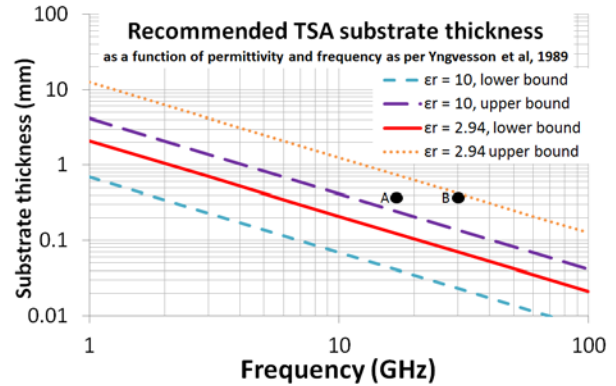

Fig. 2. Upper and lower bounds to Yngvesson's recommended range for a substrate thickness t_{eff} of $\varepsilon_r = 10$ (alumina) and 2.94 (Rogers RT/Duroid 6002). Points are marked for 18 GHz (A) and 30 GHz (B) for a 0.381 mm alumina substrate.

A. SIW parameters

Using standard waveguide equations [18], the cut-off frequency of the SIW circuit with $\varepsilon_r = 10$ and $W_{siw} = 3.6$ mm can be analyzed by computing $W_{siweff} = 3.138$ mm, the width of an equivalent waveguide section with the same ε_r. For a cut-off frequency of 15.1 GHz in alumina, the equivalent TE_{10} waveguide has a width $a = 3.141$ mm. This allows for single-mode operation up to 30.2 GHz.

B. Taper

The taper is basically linear, with opening rate R = 0.05 and shape determined by $z = c_1 e^{Ry} + c_2$ where c_1 and c_2 are the coordinates of the first and last points of the exponential.

C. Simulation setup

The coordinate system is oriented so that the substrate is in the y-z plane with x being the transverse direction (height), z is the propagation direction. As per convention, φ is measured from x in the x-y plane and θ is measured from z. Because the electric field vector is perpendicular to the metal faces, it is oriented in the x direction in the SIW

region and in the y-direction at the aperture as the tapers transition to free space (c.f. Fig. 1, bottom). Thus the E-plane is y-z at $\varphi = 90°$ and the H-plane is x-z at $\varphi = 0°$. Table 2 outlines eight designs varying substrate width W_{sub}, aperture width W_{aper}, total length L_{ant}, metal crossover point z_{met}, and substrate cut length z_{sub}, defined in Fig. 1 and depicted in Fig. 3.

Table 2: Antenna dimensions in mm for designs 1 through 8 as defined in Fig. 1. $\lambda_0 = 12.5$ mm, the free space wavelength at mid-band, i.e., 24 GHz. $\lambda_{er} = 4.0$ mm, the wavelength in alumina dielectric.

	W_{sub}	W_{aper} (λ_0)	L_{ant} (λ_{er})	z_{met}	z_{sub}
1	10.2	5.8 (.46)	89.7 (22.7)	27.6	51.2
2	11.2	6.8 (.54)	89.7 (22.7)	27.6	51.2
3	12.4	8.0 (.64)	89.7 (22.7)	27.6	51.2
4	11.6	8.0 (.64)	89.7 (22.7)	27.6	51.2
5	11.6	8.0 (.64)	62.8 (15.9)	19.3	35.9
6	11.6	8.0 (.64)	44.0 (11.1)	13.5	25.1
7	11.6	8.0 (.64)	30.8 (7.8)	9.5	17.6
8	11.6	8.0 (.64)	21.5 (5.4)	6.6	12.3

Designs 1 to 4 vary based on the aperture opening W_{aper} and the antenna width W_{sub} (c.f. Fig. 1) while keeping the antenna length L_{ant} constant at 89.7 mm. Designs 5 to 8 vary based on the L_{ant} from 89.7 mm to 21.5 mm, with the widths $W_{aper} = 8$ mm and $W_{sub} = 11.6$ mm held constant. Design 1 was modeled after Dousset [19]. In all designs, the goal is to achieve constant gain, constant beam width, and symmetric beams, along with keeping the input return loss and the cross-polarization as good as possible.

Ansoft HFSS finite-element solver (FEM) and CST microwave studio time domain finite integration technique solver (FIT) are used to calculate the S-parameters, far-field gain, HPBW, and cross-polar levels. The spherical coordinate system with Ludwig 3 polarization definition is used [20]. Comparing field solvers results in similar input return loss characteristics are shown in Fig. 4.
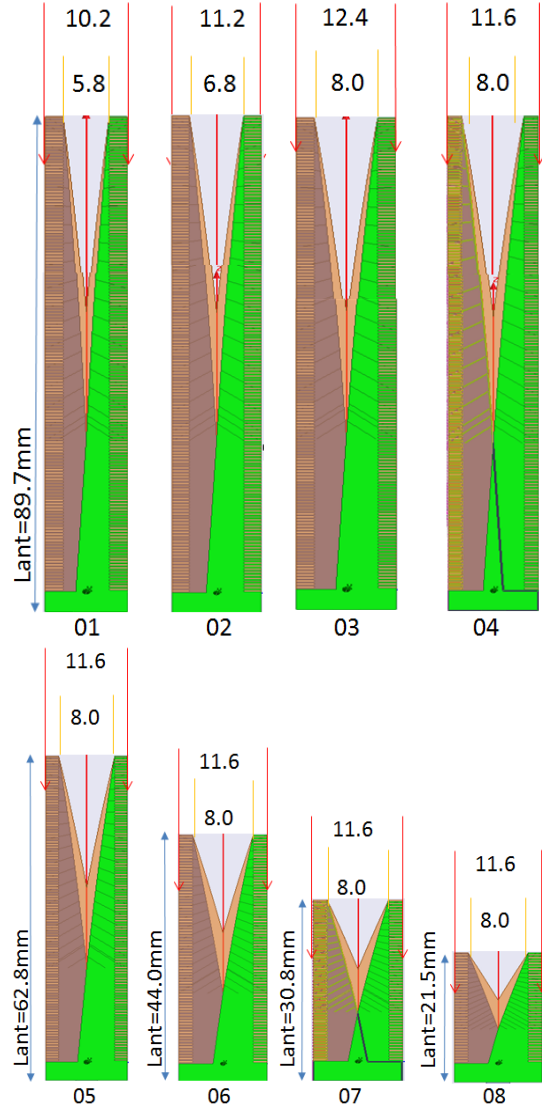

Fig. 3. LTSA dimensions for designs 1 through 8. W_{sub}: the antenna width is the upper number (mm). W_{aper}: the opening aperture width is the lower number (mm).
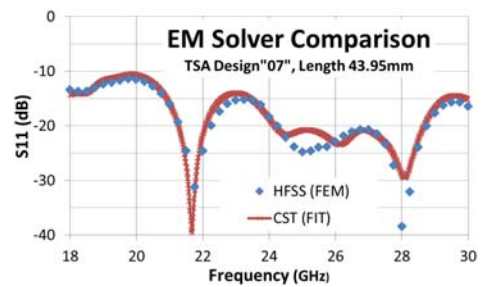

Fig. 4. Field solver comparison for design 7.

III. RESULTS

A. Input return loss

The input return loss is measured at the waveguide port, and the results incorporate both the feed and the antenna element. As seen in Fig. 5, the input return loss values for designs 1 to 4 are very similar, trending from -12 dB to -25 dB at the band edges.
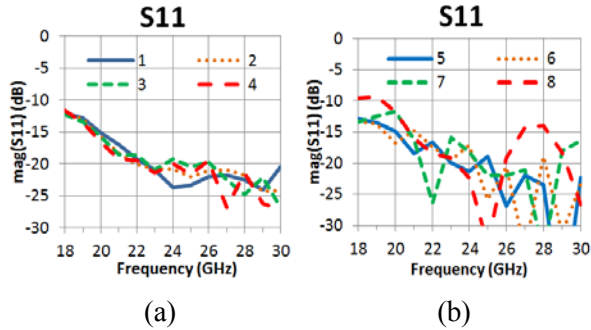

(a)   (b)

Fig. 5. Input return loss versus frequency, designs (a) 1 to 4 and (b) 5 to 8.

For the shorter length designs 5 to 8, the return loss stays below -15 dB from 21 GHz to 30 GHz except for the shortest; design 8 rises to -14 dB at the upper edge of the band. Over 18 GHz to 30 GHz, designs 1 to 5 have input return loss values better than -15 dB for 20 GHz to 30 GHz.

B. Gain

The first design goal is a flat co-polar gain response throughout the 18 GHz to 30 GHz band. Figure 6 shows designs 1 to 4 having gains varying at least 3 dB with a positive gain slope. Varying the width produces minimal change to the gain response. However, the shorter lengths in designs 6 to 8 show an increased gain at low frequencies and remarkably flat gain curves. The least variation with frequency is achieved by design 7 with only 0.8 dB (9 % of mean value, 9.23 dB) followed closely by design 8 with 1.1 dB (12 % of mean value 9.00 dB) variation. Decreasing the length beyond that of design 8 reduces the gain significantly, which is not recommended.

C. Beam width

The second goal is a constant beam width in E- and H-planes versus frequency. Gazit in [21] indicates that the radiation mechanism, aperture or travelling wave, is dependent on the opening aperture width, W_{aper}. When $W_{aper} > 2\lambda$, the antenna

operates as a travelling wave antenna. For $W_{aper} < 2\lambda$ the antenna operates as an aperture antenna and the E- and H-plane beam widths decrease with frequency. All designs from 1 to 8 are within the aperture antenna region and, as expected, the half-power beam widths generally decrease with frequency.
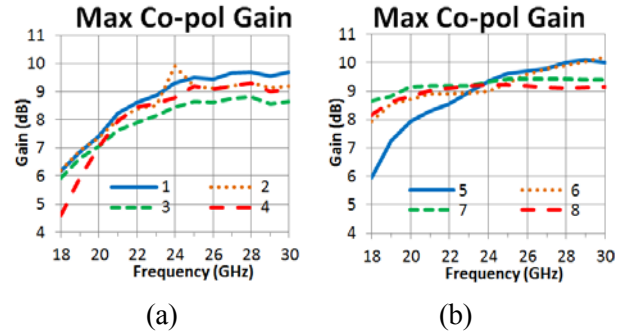

(a)   (b)

Fig. 6. Co-polar gain versus frequency for designs (a) 1 to 4 and (b) 5 to 8 at $\theta = 0°$. Flattest gain is design 7 with 0.8 dB variation across the band.

For each design, the E-plane ($\varphi = 90°$, $\theta = 0°$) HPBW is shown in Fig. 7 and H-plane ($\varphi = 0°$, $\theta = 0°$) HPBW is shown in Fig. 8. The flattest beam width versus frequency is achieved by design 7. The average HPBW over frequency and percent variation is: E-plane $49° \pm 3.2°$, 13 %, and H-plane $69° \pm 2.5°$, 7 %. However, the most symmetric is design 1: E-plane $41.3° \pm 7.5°$ and H-plane $45.1° \pm 10.6°$. E- to H-plane HPBW ratios as a function of design number are shown in Fig. 9. A ratio of 1.0 represents a perfectly symmetric beam with equal E- and H- beam widths. Design 1 has the most symmetric beam at $HPBW_E/HPBW_H = 0.91$ and the least symmetric beam is for design 8 at 0.65.
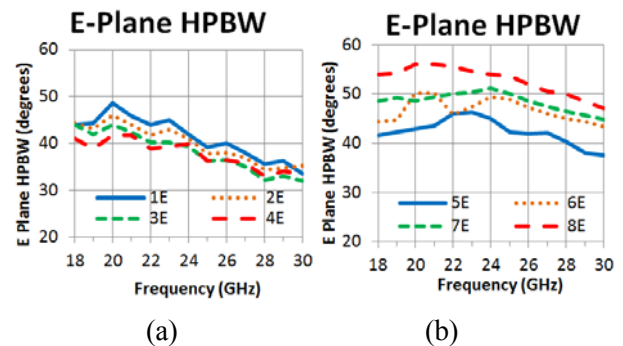

(a)   (b)

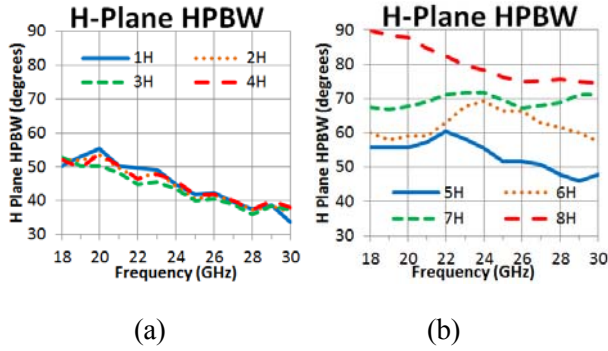Fig. 7. E-plane HPBW for designs (a) 1 to 4 and (b) 5 to 8.

(a)　　　　　　　　(b)

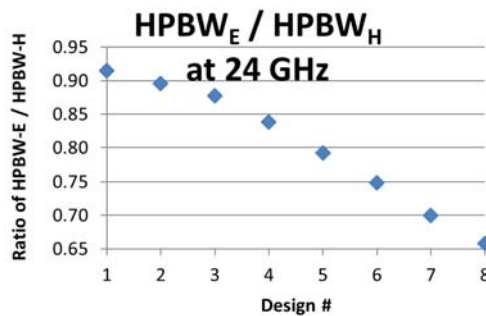Fig. 8. H-plane HPBW for designs (a) 1 to 4 and (b) 5 to 8.

Fig. 9. A measure of the beam symmetry for the E-to H-plane HPBW ratio.

D. Effect of corrugations

The metal top and bottom faces have corrugated cuts placed axially along the outside length of the antenna. The mid-band far field gain patterns versus θ for the three principle planes E (φ = 90°), D (φ = 45°) and H (φ = 0°), with and without corrugations are shown in Fig. 10 for design 1 and Fig. 11 for design 7; summarized results are in Table 3.

As with Sato's Fermi antenna with corrugations [22], a parallel mode is seen in the current phase distribution along the taper and on the outer edges of the antenna. This mode is reduced when using corrugations, leading to improved input return loss and cross-polarization levels.

Although the corrugation effects on radiation patterns are only shown for designs 1 and 7, in every design the presence of corrugations increases the bore sight gain, improved cross-polarization response and reduced S11 are shown in Fig. 12. The combination of the increased on-axis gain and the reduced D-plane cross-polarization values off-axis

significantly widens the useable beam width, which are free of cross-polarization, up to scan angles of ± 30°. Comparing the performances of designs 1 to 8, it is concluded that design 7 provides the best compromise towards an ultra-wideband, flat beam width, flat gain, and low return loss performance. However, it should be noted that design 1 presents an alternative solution with the most symmetric beam, ideal for imaging systems requiring efficient illumination of a reflector or lens. Cross-polarization levels of 28.2 dB at 18 GHz, 14.7 dB at 30 GHz and a maximum return loss of -12.0 dB are on par with design 7. The small positive gain slope (6.2 dB to 9.7 dB) of this antenna design can be cancelled out in the receiver chain.
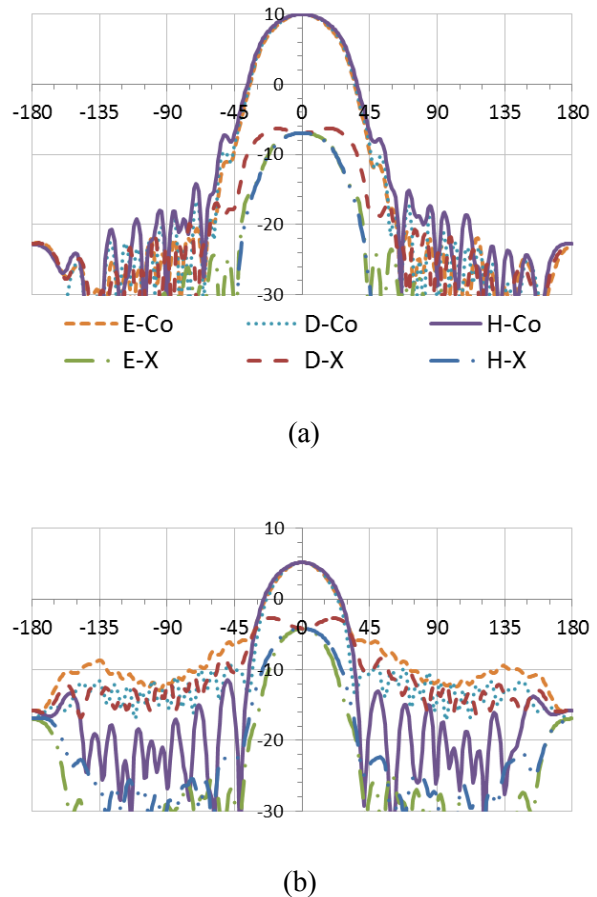

(a)

(b)

Fig. 10. Far field gain patterns versus θ in degrees, 24 GHz, design, for (a) with corrugations and (b) without corrugations; showing both co- (Co) and cross- (X) polarizations.
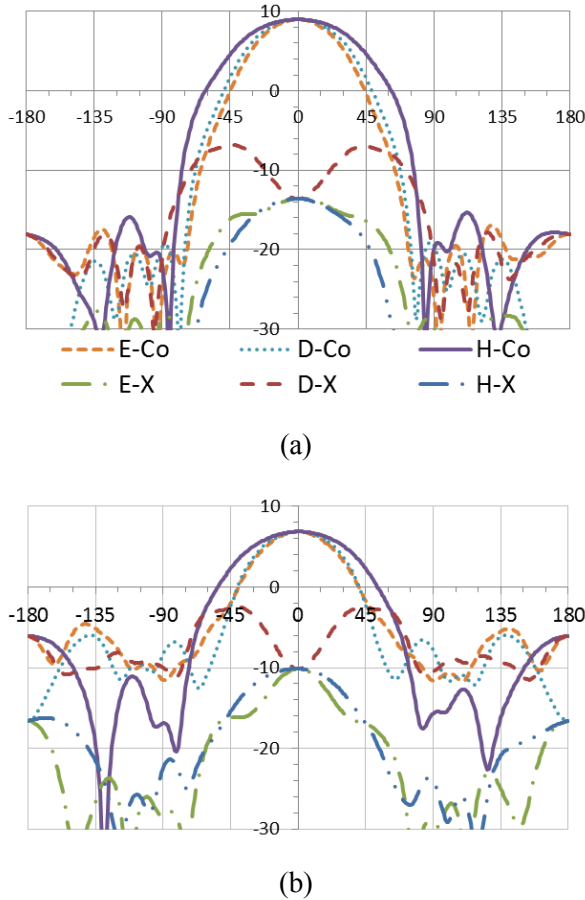
(a)

(b)

Fig. 11. Far field gain patterns versus θ in degrees, 24 GHz, design 7, for (a) with corrugations and (b) without corrugations; showing both co- (Co) and cross- (X) polarizations.
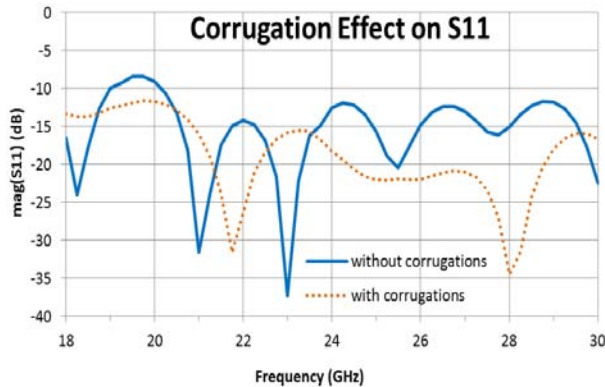

Fig. 12. Corrugation effect on the input return loss versus frequency in GHz for design 7. All designs show similar improvement with corrugations.

Table 3: Radiation pattern data from Figs. 10 and 11, with and without corrugations. The cross-polarization free beam width in the D-plane: Co-pol–X-pol $\geq 10°$.

	Design 1		Design 7	
Corrugations?	**Yes**	**No**	**Yes**	**No**
Cross-pol (dB) at boresight	19.6	13.5	33.4	16.7
Peak Gain (dB)	1.0	0.3	6.7	9.2
HPBW E-plane	43°	33°	51°	51°
HPBW H-plane	42°	33°	57°	54°
HPBW D-plane	45°	36°	71°	66°
HPBW symmetry $HPBW_E/HPBW_H$	0.92	0.91	0.71	0.70
Cross-pol free Beam width	<1°	60°	40°	72°

IV. CONCLUSION

A planar antipodal TSA element for use in the ultra-wide extended K Band, 18 GHz - 30 GHz with SIW input feed network is selected from a parametric study. The design uses ceramic alumina substrate and takes advantage of regular corrugations along the outside axial length of the antenna. Simulation results of design 7 show a 12 % gain variation, 13 % and 7 % HPBW variations in the E- and H-planes, respectively, over the band. Cross-polarization levels at the bore sight vary from 35.7 dB at 18 GHz to 17.4 dB at 30 GHz, and the return loss stays below -11.7 dB. Alternatively, design 1 has excellent beam symmetry ($HPBW_E/HPBW_H = 0.91$) and cross-polarization (19.6 dB at 24 GHz) and would be ideal for efficiently illuminating a focusing element such as a reflector or lens. Thus both LTSA designs 1 and 7 presented show excellent performance for ultra-wideband dual-polarization focal plane array feed applications.

ACKNOWLEDGMENT

REFERENCES

[1] H. Holter, T. -H. Chio, and D. Schaubert, "Experimental results of 144-element dual-polarized endfire tapered-slot phased arrays," *IEEE Trans. Antennas Propagat.*, vol. 48, pp. 1707-1718, 2000.

[2] W. A. van Cappellen and L. Bakker, "APERTIF: phased array feeds for the Westerbork synthesis radio telescope," *IEEE Int. Symp. Phased Array Systems Tech.*, pp. 640-647, Waltham, MA, Oct. 2010.

[3] B. Veidt, G. Hovey, T. Burgess, R. Smegal, R. Messing, A. Willis, A. Gray, and P. Dewdney, "Demonstration of a dual-polarized phased-array feed," *IEEE Trans. Antennas Propagat.,* vol. 59, pp. 2047-2057, 2011.

[4] P. Gibson, "The Vivaldi aerial," *Proc. 9th European Microwave Conf.*, pp. 101-105, Brighton, UK, June 1979.

[5] K. Yngvesson, D. Schaubert, T. Korzeniowski, E. Kollberg, T. Thungren, and J. Johansson, "Endfire tapered slot antennas on dielectric substrates," *IEEE Trans. Antennas Propagat.*, vol. 33, pp. 1392-1400, 1985.

[6] K. S. Yngvesson, T. L. Korzeniowski, Y. -S. Kim, E. Kollberg, and J. F. Johansson, "The tapered slot antenna - A new integrated element for millimeter wave applications," *IEEE Trans. on Microwave Theory Tech.*, vol. 37, pp. 365-374, Feb. 1989.

[7] M. W. Elsallal and J. C. Mather, "An ultra-thin, decade (10:10) bandwidth, modular "BAVA" array with low cross-polarization," *IEEE AP-S Int. Symp. Dig.*, pp. 1980-1983, Spokane, WA, July 2011.

[8] S. Sugawara, Y. Maita, K. Adachi, K. Mori, and K. Mizuno, "A mm-wave tapered slot antenna with improved radiation pattern," *IEEE MTT-S Int. Microwave Symp. Dig.*, pp. 959-962, Denver, CO, June 1997.

[9] C. -M. Hsu, L. Murphy, T. -L. Chin, and E. Arvas, "Vivaldi antenna for GPR," *Proc. ACES Conf.*, pp. 490-494, Monterey, CA, Mar. 2009.

[10] T. Namas and M. Hasanovic, "Ultrawideband antipodal Vivaldi antenna for road surface scanner based on inverse scattering," *Proc. ACES Conf.*, pp. 882-887, Monterey, CA, Apr. 2012.

[11] Z. -L. Zhou, L. Li, J. -S. Hong, and B. -Z. Wang, "A novel harmonic suppression antenna with both compact size and wide bandwidth," *ACES Journal*, vol. 27, pp. 435-440, May 2012.

[12] W. O'Keefe Coburn and A. I. Zaghloul, "Wire realization of a tapered slot antenna with reconfigurable elements," *Proc. ACES Conf.*, pp. 324-329, Monterey, CA, Mar. 2011.

[13] D. Deslandes and K. Wu, "Integrated microstrip and rectangular waveguide in planar form," *IEEE Microwave Wireless Comp. Lett.*, vol. 11, pp. 68-70, Feb. 2001.

[14] D. Deslandes, "Design equations for tapered microstrip-to-substrate integrated waveguide transitions," *IEEE MTT-S Int. Microwave Symp. Dig.*, pp. 707-707, Anaheim, CA, 2010.

[15] F. Taringou and J. Bornemann, "New substrate-integrated to coplanar waveguide transition," *Proc. 41st European Microwave Conf.*, pp. 428-431, Manchester, UK, 2011.

[16] N. Fourikis, N. Lioutas, and N. Shuley, "Parametric study of the co- and cross-polarisation characteristics of tapered planar and anitpodal slotline antennas," *IEE Proc. Microw. Antennas Propag.*, vol. 140, pp. 17-22, Feb. 1993.

[17] S. Sugawara, Y. Maita, K. Adachi, K. Mori, and K. Mizuno, "Characteristics of a mm-wave tapered slot antenna with corrugated edges," *IEEE MTT-S Int. Microwave Symp. Dig.*, pp. 533-536, Baltimore, MD, June 1998.

[18] L. Yan, W. Hong, G. Hua, J. Chen, K. Wu, and T. Cui, "Simulation and experiment on SIW slot array antennas," *IEEE Microwave Wireless Comp. Lett.,* vol. 14, pp. 446-448, Sep. 2004.

[19] D. Dousset, *Développement de Composants SIW dans la Bande 3 d'ALMA (84-116 GHz) et Conception d'une Jonction Orthomode (OMT) dans la Bande 1 d'ALMA (31-45 GHz) en Technologie Guide d'onde*, Ph.D. dissertation, École Polytechnique de Montréal, Montreal, Canada, Aug. 2010.

[20] A. Ludwig, "The definition of cross-polarisation," *IEEE Trans. Antennas Propag.*, vol. 21, pp. 116-119, 1973.

[21] E. Gazit, "Improved design of the Vivaldi antenna," *IEE Proc. Microw. Antennas Propag.*, vol. 135, pp. 89-92, Apr. 1988.

[22] H. Sato, K. Sawaya, N. Arai, Y. Wagatsuma, and K. Mizuno, "Broadband FDTD analysis of Fermi antenna with narrow width substrate," *IEEE AP-S Int. Symp. Dig.*, pp. 261-264, Columbus, OH, June 2003.

Lisa Shannon Locke was born in the Northwest Territories, Canada. She received the B.Sc. degree in Electrical Engineering from the University of Alberta, Edmonton, AB, Canada in 1997 and a M.Sc. degree in Electrical Engineering in 2001 from the University of Cape Town, South Africa. She worked as a student engineer for the California Institute of Technology on a K-band water vapor radiometer at the millimeter array at Owens Valley Radio Observatory in 1996. She continued work on water vapor radiometers at the National Radio

Astronomy Observatory, Green Bank, WV on a 86-GHz tipping radiometer and the prime-focus L-band receiver for the Green Bank Telescope. For five years she was with the receiver group at the National Astronomy and Ionosphere Center's Arecibo Observatory in Puerto Rico. In 2005 she joined the National Radio Astronomy Observatory, Socorro, NM where she was involved with the upgrade of cryogenic receiver front-ends for the expanded very large array (EVLA).

Currently she is working on a PhD degree in electrical engineering at the University of Victoria, BC, Canada and the Hertzberg Institute of Astrophysics, Victoria, BC in the field of focal plane array antennas.

Jens Bornemann received the Dipl.-Ing. and the Dr.-Ing. degrees, both in Electrical Engineering, from the University of Bremen, Germany, in 1980 and 1984, respectively. From 1984 to 1985, he was a consulting engineer. In 1985, he joined the University of Bremen, Germany, as an Assistant Professor. Since April 1988, he has been with the Department of Electrical and Computer Engineering, University of Victoria, Victoria, B.C., Canada, where he became a Professor in 1992. From 1992 to 1995, he was a Fellow of the British Columbia Advanced Systems Institute. In 1996, he was a Visiting Scientist at Spar Aerospace Limited (now MDA Space), Ste-Anne-de-Bellevue, Québec, Canada, and a Visiting Professor at the Microwave Department, University of Ulm, Germany. From 1997 to 2002, he was a co-director of the Center for Advanced Materials and Related Technology (CAMTEC), University of Victoria. From 1999 to 2002, he served as an Associate Editor of the *IEEE Transactions on Microwave Theory and Techniques* in the area of Microwave Modeling and CAD. In 2003, he was a Visiting Professor at the Laboratory for Electromagnetic Fields and Microwave Electronics, ETH Zurich, Switzerland. He has coauthored *Waveguide Components for Antenna Feed Systems. Theory and Design* (Artech House, 1993) and has authored/coauthored more than 250 technical papers. His research activities include RF/wireless/microwave/millimeter-wave components and systems design, and field-theory-based modeling of integrated circuits, feed networks and antennas.

Dr. Bornemann is a Registered Professional Engineer in the Province of British Columbia, Canada. He is a Fellow IEEE, a Fellow of the Canadian Academy of Engineering and served on the Technical Program Committee of the *IEEE MTT-S International Microwave Symposium* and the Editorial Boards of the *International*

Journal of Numerical Modeling and the *International Journal of Electronics and Communication (AEÜ)*.

Stéphane Claude received the Engineering degree in material sciences from the Ecole Nationale Supérieure d'Ingénieurs de Caen, France, 1990 and the PhD degree in Physics from London University, Queen Mary and Westfield College, London, UK, 1996. From 1990 to 1996, he was a research associate at the Rutherford Appleton Laboratory, U.K., where he developed techniques for the fabrication of Superconducting-Insulator-Superconducting (SIS) mixer chips, for low noise sub-millimeter receivers in Radio-Astronomy. Part of his PhD work was to commission a 500 GHz receiver at the James Clerk Maxwell Telescope (JCMT), Hawaii. In 1996 he joined the Herzberg Institute of Astrophysics, B.C., Victoria, Canada where he continued development on low noise receivers for astronomy, including a 200 GHz receiver for the JCMT and a sideband separating mixer design. From 2000 to 2002 he joined the Institut de Radioastronomie Millimétrique (IRAM), Grenoble, France, where he worked on the design of a 275-370 GHz receiver (Band 7) for the Atacama Large Millimetre Array (ALMA). Since 2002, he has been leading the millimeter instrumentation team at the Herzberg Institute of Astrophysics, Victoria, B.C. He was project engineer for the 84-116 GHz receiver (Band 3) developed for the ALMA. He is also adjunct professor at the University of Victoria, Victoria, B.C., Canada. His research interests include millimeter-wave low noise receivers and phased array feeds for radio astronomy.